Chemistry & Biology
Article

Sanguinarine Interacts with Chromatin, Modulates Epigenetic Modifications, and Transcription in the Context of Chromatin

Ruthrotha Selvi B,[1,3] Suman Kalyan Pradhan,[2,3] Jayasha Shandilya,[1] Chandrima Das,[1] Badi Sri Sailaja,[1] Naga Shankar G,[1] Shrikanth S. Gadad,[1] Ashok Reddy,[1] Dipak Dasgupta,[2,*] and Tapas K. Kundu[1,*]
[1]Transcription and Disease Laboratory, Molecular Biology and Genetics Unit, Jawaharlal Nehru Centre for Advanced Scientific Research, Jakkur, Bangalore 560064, India
[2]Biophysics Division, Saha Institute of Nuclear Physics, Block-AF, Sector-I, Bidhannagar, Kolkata 700 064, India
[3]These authors contributed equally to this work.
*Correspondence: dipak.dasgupta@saha.ac.in (D.D.), tapas@jncasr.ac.in (T.K.K.)
DOI 10.1016/j.chembiol.2008.12.006

SUMMARY

DNA-binding anticancer agents cause alteration in chromatin structure and dynamics. We report the dynamic interaction of the DNA intercalator and potential anticancer plant alkaloid, sanguinarine (SGR), with chromatin. Association of SGR with different levels of chromatin structure was enthalpy driven with micromolar dissociation constant. Apart from DNA, it binds with comparable affinity with core histones and induces chromatin aggregation. The dual binding property of SGR leads to inhibition of core histone modifications. Although it potently inhibits H3K9 methylation by G9a in vitro, H3K4 and H3R17 methylation are more profoundly inhibited in cells. SGR inhibits histone acetylation both in vitro and in vivo. It does not affect the in vitro transcription from DNA template but significantly represses acetylation-dependent chromatin transcription. SGR-mediated repression of epigenetic marks and the alteration of chromatin geography (nucleography) also result in the modulation of global gene expression. These data, conclusively, show an anticancer DNA binding intercalator as a modulator of chromatin modifications and transcription in the chromatin context.

INTRODUCTION

Sanguinarine (13-methyl[1,3]benzodioxolo[5,6-c]-1,3-dioxolo [4, 5-i] phenanthridium), a plant alkaloid, is derived from the root of *Sanguinaria canadensis, Argemone mexicana*, and other poppy-fumaria species (Shamma and Guinaudeau, 1986). It possesses antimicrobial, antioxidant, anti-inflammatory, and proapoptotic properties (Malikova et al., 2006; Adhami et al., 2003; Mandel, 1994). It is a potent inhibitor of nuclear factor κB (NF-κB) activation and consequent cell growth and survival (Chaturvedi et al., 1997). SGR blocks proliferation and induces apoptosis in different malignant cell types (Hussain et al., 2007; Adhami et al., 2003). It induces cell cycle arrest at the G_0/G_1 phase (Adhami et al., 2004). These effects originate from the ability of SGR to target a variety of cellular components (Wolff and Knipling, 1993; Vogt et al., 2005; Barreto et al., 2003; Wang et al., 1997; Straub and Carver, 1975; Vallejos, 1973; Ulrichova et al., 2001).

The cationic form of the drug at pH 6.5 binds reversibly to B DNA with GC base preference via intercalation (Maiti et al., 2002; Das et al., 2003; Maiti and Kumar, 2007). Although in recent years extensive investigation is being done to understand the basis of potential antineoplastic activity of SGR, the molecular target(s) is yet to be identified. Its potent antiproliferative and DNA intercalation property prompted us to investigate the interaction of the drug with chromatin and the structure-function consequences thereof.

As a first step, we have estimated the binding parameters and associated energetics of the association at different levels of chromatin structure by means of fluorescence, circular dichroism (CD) spectroscopy, and isothermal titration calorimetry (ITC). The trend in the change of enthalpy with the temperature (heat capacity changes) for binding has given information about the structural alterations of the chromatin, mononucleosome, and chromosomal DNA consequent to the association. CD spectroscopy was used as the preliminary probe for SGR-induced structural alterations. We have probed the SGR induced alteration in the size distribution of chromatin and mononucleosome by means of dynamic light scattering. Moreover, confocal and atomic force microscopy have been used for direct visualization of the ligand-induced alteration of the in vivo chromatin organization. We have also noticed that in addition to DNA, SGR binds to the core histones with comparable affinity. Furthermore, we have addressed the effect of chromatin structure perturbation and the histone binding potential of SGR on the dynamicity of chromatin that modulates the different DNA-templated phenomena in the cell. There are several factors that contribute to the chromatin dynamics, including posttranslational modifications of chromatin associated proteins (histones and nonhistones) and ATP-dependent chromatin remodeling machinery (Kouzarides, 2007; Hogan and Varga-Weisz, 2007). Among the different posttranslational modifications, reversible acetylation, phosphorylation, and methylation are directly involved in the regulation of gene expression (Kouzarides, 2007).

Dysfunction of chromatin modification is causally related to the cancer manifestation (Jones and Baylin, 2007). For example, hyperacetylation of histones (Van Beekum and Kalkhoven, 2007), mistargeting/misregulation of histone deacetylases (Nakagawa et al., 2007) and acetyltransferases (Rothhammer and Bosserhoff, 2007), overexpression of histone kinases (Oki et al., 2007), and alteration of the histone methyltransferases and tumor suppressor interactions (Tonini et al., 2008) are commonly documented in different cancer manifestation. Thus, these chromatin modifying enzymes are being considered as new-generation therapeutic targets for cancer therapy (Swaminathan et al., 2007).

Remarkably, we have found that SGR inhibits histone methylation with an inherent specificity toward lysine and arginine methylation linked to transcriptional activation. It is a potent inhibitor of histone acetylation (HATs) in vitro and in vivo, as observed in cell lines and mouse liver. Although SGR intercalates into DNA base pairs, when it binds to DNA devoid of histones it does not apparently inhibit the transcription from DNA template. In contrast, it inhibits the p300-HAT-dependent chromatin transcription. However, the physiologically relevant concentration for the inhibition of histone acetylation does not induce proapoptotic gene expression, thereby indicating that the interaction of SGR with different chromatin components leading to inhibition of histone modifications is independent of its well-documented role in apoptotic pathway. This was further verified by examining the global gene expression profile of cells treated with both low and high concentrations of SGR. We observe a differential pattern of gene regulation based on the dosage. The treatment with a low concentration for a shorter duration results in about 55% downregulation of genes. However, when the dosage is increased, upregulation of gene expression is much more profound. The results, in totality, might provide a new direction for the molecular mechanisms of action of DNA intercalators with anticancer properties, particularly those with dual binding ability to DNA and core histones. It also suggests the possible targeting of multiple enzymes by a single molecular species, especially in the area of antineoplastic therapeutics.

RESULTS

Characterization of SGR Association with Chromatin

Sanguinarine is an established intercalator class of DNA-binding alkaloid (Figure 1A), with high cell permeability potential. Although substantial work has been done regarding the effect of SGR on different cell lines and in an animal model (Adhami et al., 2004; Dvorak and Simanek, 2007), surprisingly no report is available about its interaction with chromatin and its constituent components such as histones. Association of SGR with chromatin, mononucleosome, and chromosomal DNA (subsequently denoted as polymers) was probed by fluorescence spectroscopy. Blue shift of emission maximum of SGR with a concomitant decrease in quantum yield in the fluorescence spectrum is the preliminary evidence for the binding of SGR with different levels of chromatin structure (polymers) (see Figure S1 available online). Both are dependent on the nature of the polymer. The binding isotherms generated from fluorescence measurements suggest noncooperative association (Figure 1B). Corresponding dissociation constants evaluated from nonlinear curve fitting of binding isotherms are summarized in Table 1. The value of the binding stoichiometry and dissociation constant for association of SGR with HeLa chromatin are 6 bases per SGR and 8 μM, respectively, which is in good agreement with the similar values for rat liver chromatin (Table 1). The dissociation constant value for chromosomal DNA is of the same order as reported earlier for calf thymus DNA and synthetic polynucleotide (Das et al., 2003), thereby supporting the results obtained from the fluorescence method.

The local electronic environment of SGR during its interaction with different chromatin components was probed by means of excited state lifetime measurements of the SGR fluorophore. Fluorescence decays could be fitted with a biexponential function. Mean lifetime decreases in the order: chromosomal DNA (10.6 ns) > chromatin (8.8 ns) > mononucleosome (6.3 ns). The decay profile of free SGR in Tris-HCl buffer (pH 6.5) could be fitted well with a biexponential function with τ_1 = 2.5 ns and τ_2 = 0.15 ns. Increase in lifetime upon interaction with polymers could be attributed to an increase in hydrophobicity of the microenvironment originating from intercalation of SGR within DNA base pairs (Prendergast, 1991). However, dependence of the lifetime upon association of DNA with histones in chromatin and mononucleosome implies a difference in their local environment of SGR fluorophore. In case of chromatin and mononucleosome, the physical environment from associated proteins, especially histones, could be the other plausible source of enhanced lifetime. To test our hypothesis, we investigated the possibility of interaction of SGR with core histones by fluorescence spectroscopy. Quenching of SGR fluorescence accompanied by blue shift provides the direct physical evidence for the association of histones with SGR (Figure 2B). Nonlinear curve fitting analysis of the noncooperative binding isotherm yields the dissociation constant (K_d) value of 8.8 μM.

Isothermal calorimetric titrations were performed to evaluate the binding parameters and associated energetics of SGR-polymer binding. A representative titration thermogram and binding isotherm for SGR-chromatin association are shown in Figure 1C. Dissociation constants and binding stoichiometry values obtained from ITC measurements compare well with those estimated from fluorescence titration (Table 1). Association is enthalpy driven in all cases. Variation of enthalpy and entropy with temperature decreases in order: mononucleosome > chromatin > chromosomal DNA (Figures 1D and 1E). Taken together, these results suggest that SGR not only binds to DNA, but it also interacts with core histone component of chromatin with comparable affinity.

Sanguinarine Induces Conformational Changes by Interacting with Chromatin

The effect of SGR on the structure of native chromatin, mononucleosome, and chromosomal DNA was examined by CD spectroscopy. Spectra for native chromatin, mononucleosome, and chromosomal DNA agree well with previous reports (Murcia et al., 1978; Vergani et al., 1994). Optically inactive SGR (400 nm to 220 nm) exhibits positive induced band upon intercalation within DNA base pairs (Das et al., 2003). Emergence of induced CD band (310–380 nm) thus demonstrates SGR-polymer association. Relevant spectra are shown in Figure 2A (panels I, II, and III). Because the induced band originates from optically asymmetric

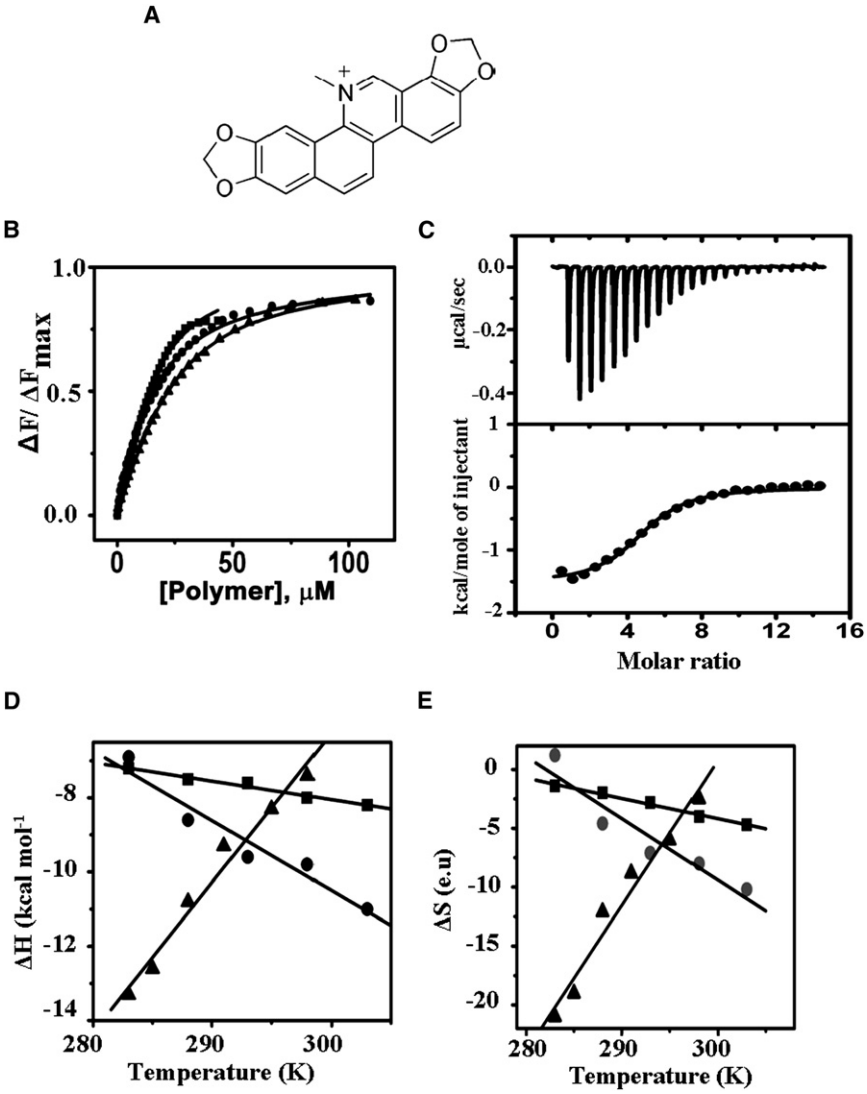

Figure 1. SGR Interacts with Histones

(A) Structure of SGR.

(B) Curve-fitting analyses to evaluate the dissociation constant for the association of SGR with different levels of chromatin structure: chromatin (○), mononucleosome (Δ), and chromosomal DNA (□) in 10 mM Tris-HCl (pH 6.5) at 25°C. Dissociation constant values obtained from the fitting of the binding isotherms by the nonlinear least-squares method are 10 μM, 12 μM, and 17 μM for chromosomal DNA, chromatin, and mononucleosome, respectively. The concentration of SGR taken was 5 μM in all three cases.

(C) Exchange of heat of association of SGR with chromatin. Upper panel is the isothermal calorimetric titration of 1.2 mM chromatin into 10 μM SGR at 25°C in 10 mM Tris-HCl buffer (pH 6.5). Lower panel is the exothermic heat exchanged per mole of injectant as a function of molar ratio of chromatin to SGR. The data were fitted with the "one set of sites" binding model. Solid line represents the fit of the binding isotherm.

(D) Temperature dependence of calorimetric enthalpy of association between SGR and chromatin (○), mononucleosome (Δ), and chromosomal DNA (□). The lines represent the fits of data to equation $\Delta H\ (T) = \Delta H\ (T_0) + \Delta Cp^*(T\text{-}T_0)$. Values of ΔC_p obtained from the fits are −0.2, −0.09, and + 0.40 kcal mol^{-1} K^{-1} for chromatin, chromosomal DNA, and mononucleosome, respectively.

(E) Temperature dependence of calorimetric entropy of association of SGR with different levels of chromatin structures: chromatin (○), mononucleosome (Δ), and chromosomal DNA (□).

environment from DNA and DNA-protein complexes, difference in their peak positions (Figure 2A) suggests nonidentical optical environments of SGR bound to different levels of chromatin. Marked alterations in the spectra of chromatin and mononucleosome (300 nm to 230 nm) also characterize their association with SGR. Inset I of Figure 2A shows the time-dependent decrease in the ellipticity at 272 nm, an index of chromatin aggregation. CD spectroscopic results were supported from the thermodynamic data. Magnitude of ΔC_p (calculated from the slope of linear fit of the plot ΔH versus T) is an index of the ligand-induced alteration of the polymer structure, particularly the solvent exposed surface area. Large positive ΔC_p in case of mononucleosome suggests that SGR induces its structural alteration to a significant degree (Figure 1D and Table 1). Similarly, ΔC_p for SGR-chromatin binding implies an SGR-induced radical change in chromatin structure upon association with SGR. Dynamic light scattering measurements were done to further characterize the ultrastructural consequences of SGR association with chromatin, mononucleosome, and chromosomal DNA (Figure 2C, I and II). There was a clear increase in the mean hydrodynamic diameter of chromatin in presence of SGR, suggesting that the alkaloid induces chromatin aggregation in vitro. However, SGR itself does not get aggregated in solution, as tested by ITC at different pH conditions (Figure S2). In contrast, there is no significant shift in the mean hydrodynamic diameter of mononucleosome and chromosomal DNA in presence of bound SGR. SGR-induced increase in hydrodynamic diameter implying aggregation of chromatin was also checked in vivo on HeLa cells by confocal (Figure 2D) and atomic force microscopy (Figure 2E). Unlike the untreated or dimethyl sulfoxide (DMSO, solvent) treated cells, SGR treatment leads to the aggregation of chromatin into distinct large foci (Figure 2D, I and II; Figure 2E, I; compare panels i and ii with iii). For the finer understanding of the alteration of nuclear architecture upon SGR treatment, the isolated HeLa nuclei were subjected to atomic force microscopy (AFM) analysis upon partial micrococcal nuclease digestion (Figure 2E, panel II). The untreated or DMSO-treated nuclei were found to be uniformly digested by MNase, but SGR-treated nuclei that were highly aggregated were accessible to a variable extent due to the formation of large compact chromatin domains (Figure 2E, panel II; compare iv and v with vi). These results suggest that interaction of SGR induces chromatin aggregation in the cells.

Table 1. Thermodynamic Parameters and Stoichiometry of Binding for the Association of SGR with Chromatin, Mononucleosome, and Chromosomal DNA in 10 mM Tris-HCl (pH 6.5) at 25°C

	K_d[a] (μM)	n (Bases/Drug)	ΔH (kcal/Drug)	ΔS (e.u.[e])	ΔC_P (kcal·mol^{-1}·K^{-1})
Chromatin	3.3 ± 0.3[b]	6 ± 0.5[b]	−9.8 ± 0.3[b]	−7.1 ± 0.1[b]	−0.2[b]
	12 ± 0.5[c]	6 ± 0.5[c]			
	8 ± 0.5[d]	6 ± 0.5[d]			
Mononucleosome	10 ± 0.5[b]	8 ± 0.5[b]	−7.4 ± 0.4[b]	−2.5 ± 0.2[b]	+0.4[b]
	17 ± 0.5[c]	8 ± 0.5[c]			
Chromosomal DNA	1.1 ± 0.3[b]	4 ± 0.1[b]	−8 ± 0.3[b]	−4 ± 0.1[b]	−0.09[b]
	10 ± 0.3[c]	4 ± 0.1[c]			

[a] K_d is the apparent dissociation constant ($K_d = K_0 \times n$, where K_0 is the intrinsic dissociation constant and n is the binding stoichiometry).
[b] Values were determined by the calorimetric method.
[c] Values were determined by the fluorimetric method.
[d] Represents the values for HeLa chromatin.
[e] Entropy units.

Sanguinarine Inhibits Histone Methylation with Differential In Vivo Dynamics

Previous experiments clearly suggest that SGR interacts with chromatin both through histones and DNA. Its ability to interact with the histones encouraged us to find out whether SGR alters the state of chromatin modifications. The relatively stable histone modification, methylation of lysine, and arginine residues play an important role in the different cellular functions along with other chromatin modifications. Histone methylation can be associated with both gene activation and repression based on the residue and modification status. It was observed that SGR could inhibit the lysine methyltransferase G9a-mediated histone methylation with an IC_{50} of approximately 5 μM as revealed by a filter binding assay (Figure 3A, compare lane 3 with lanes 4–7). The filter binding assay was further confirmed by fluorographic gel assay, which showed that the methylation of histone H3 by G9a was efficiently inhibited by SGR (Figure 3B). Methylation of arginine residues by PRMT4/CARM1 was also found to be inhibited by SGR, with an IC_{50} value of 10 μM both by filter binding and fluorographic gel assay (Figure 3A, compare lane 3 with lanes 4–7; Figure 3C). Inhibition of histone methylation in vivo by SGR was found to be quite interesting (see Discussion). Methylation of histone H3, at K9 was least affected in presence of 2 μM concentration of SGR in HeLa cells, as observed by western blot analysis (Figure 3D, panel I), whereas the methylation marks associated with transcriptional activation, asymmetric dimethylation of histone H3R17, and trimethylation of H3K4 were drastically inhibited by SGR at a similar concentration (2 μM) (Figure 3D, panels II and III, respectively). These results indicate that binding of SGR to chromatin inhibits H3K4 and H3R17 methylation, an epigenetic mark associated with transcriptional activation, more efficiently than H3K9 methylation, a marker for silent heterochromatin.

Sanguinarine Is a Potent Inhibitor of Histone Acetylation

Methylation of histone H3K4 and H3R17 along with the acetylation of specific sites (both in H3 and H4) marks the transcriptionally active state of a gene. Therefore, we investigated whether SGR could also modulate histone acetyltransferase activity. Interestingly, in vitro histone acetyltransferase assays using two different classes of histone acetyltransferases, p300 and PCAF, clearly showed that SGR could efficiently inhibit histone acetyltransferase activity with an approximate IC_{50} value of 10 μM (Figure 4A). Quantitative filter binding assay was further confirmed by gel fluorography assay. The results showed that 5–20 μM SGR gradually inhibited the acetylation of histones H3 and H4 very potently (Figures 4B and 4C, lanes 5–7). Because SGR is highly permeable to cells, the inhibition of histone acetylation was confirmed by western blot analysis of extracted histones from the SGR-treated cells. In agreement with the in vitro HAT assays, it was found that in presence of SGR, acetylation of histone H3 was significantly inhibited even at 2 μM concentration when treated for only 3 hr (Figure 4D compare lane 2 with lanes 3 and 4). We further investigated the transient changes in the state of histone acetylation in mice liver upon SGR treatment. Interestingly, there was a drastic reduction of histone acetylation in the liver of mice injected with SGR (25 mg/kg body weight) as compared with the solvent (DMSO) control, observed within 6 hr (Figure 4E, panel II; compare DMSO with SGR). However, the drug treatment did not induce any apparent toxicity to the animal because the morphology of the cells did not show any significant change. Taken together, these data establish SGR as a potent inhibitor of histone acetylation in vitro and in vivo.

Sanguinarine Does Not Affect the DNA Transcription but Inhibits the Acetylation-Dependent Chromatin Transcription

Sanguinarine strongly binds to DNA via intercalation and also interacts with histones, resulting in the inhibition of different chromatin modifications associated with transcriptional activation. Therefore, we were interested to find out the effect of SGR on the first level of gene expression, transcription. For this purpose, the in vitro transcription experiments were performed following the scheme depicted in Figure 5A. Interestingly, the presence of a 10–25 μM concentration of SGR did not have a significant effect on transcription from the naked DNA template (Figure 5B, compare lane 3 with lanes 4–6). However, acetylation-dependent transcription from an in vitro assembled chromatin template showed a dose-dependent inhibition in the presence of SGR (Figure 5E compare lane 3 with lanes 4–6). Further increase in the SGR concentration up to 75 μM did not affect the DNA transcription, though the transcription from the chromatin template was almost completely inhibited at similar

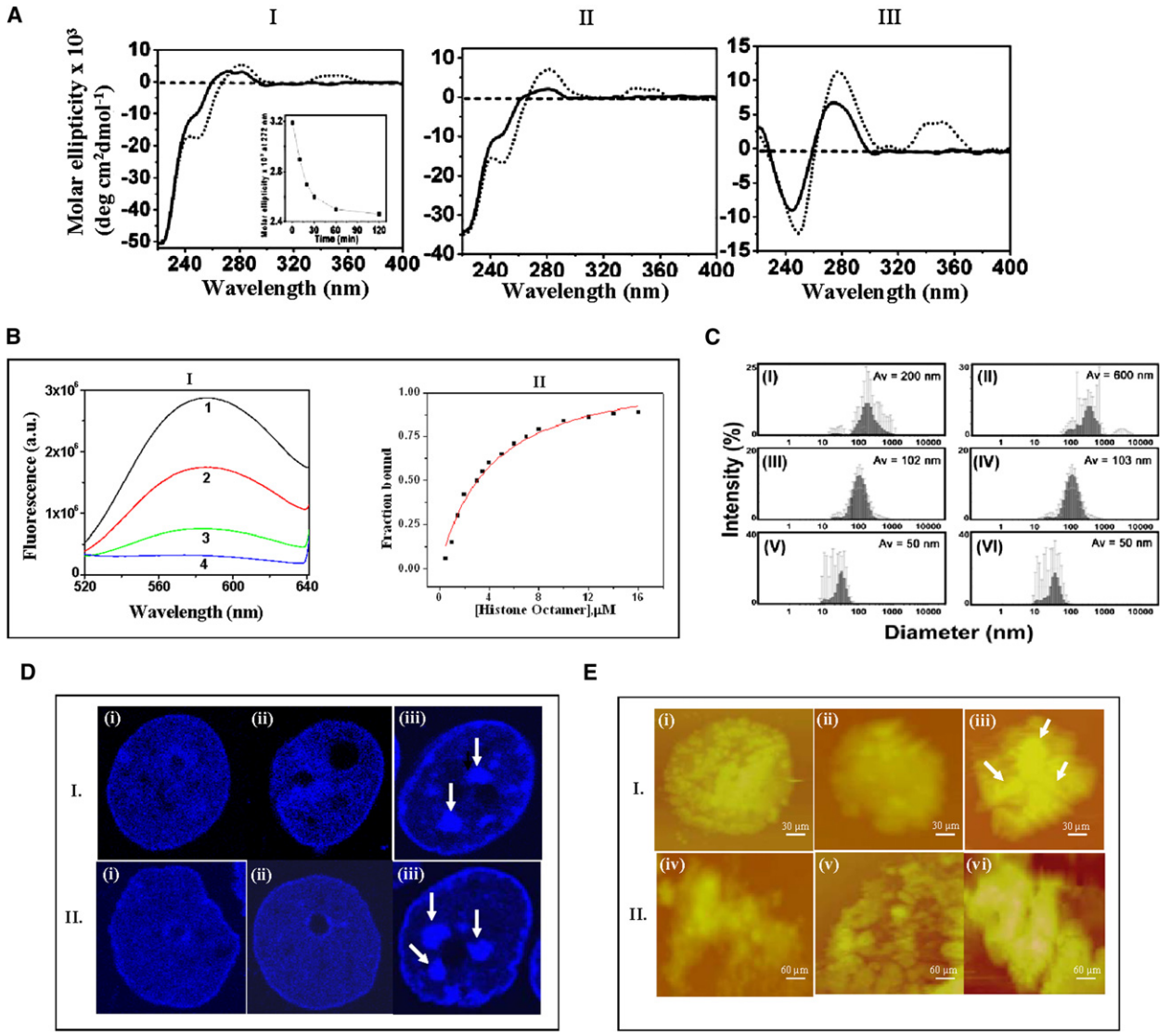

Figure 2. SGR Induces Conformational Changes upon Interacting with Chromatin

(A) Circular dichroism spectra of 10 μM SGR alone (…) and in presence of 39 μM polymer (—) in 10 mM Tris-HCl (pH 6.5) at 25°C. Panels I, II, and III correspond to chromatin, mononucleosome, and chromosomal DNA, respectively. Spectrum 2 (- - -) is the only polymer (39 μM) in all three cases. Inset of (A) is the plot of molar ellipticity value at 272 nm (θ_{272}) versus time for chromatin.

(B) Panel I: Fluorescence quenching of SGR in presence of histone octamer for SGR alone (5 μM, spectrum 1) and in the presence of octamer (5 μM, spectrum 2; 8 μM, spectrum 3; 16 μM, spectrum 4). Panel II: Best fit curve of the binding isotherm generated by nonlinear least-squares method for the association of SGR with octamer under previously mentioned conditions.

(C) Intensity distribution (%) of different levels of chromatin structure as a function of size (in diameter) obtained from DLS measurements. Figures in the left panel represent chromatin, mononucleosome, and chromosomal DNA (from top to bottom), respectively. Figures in the right panel represent corresponding polymer complexed with SGR. All experiments were done in 10 mM Tris-HCl (pH 6.5) at 25°C.

(D and E) Global chromatin organization upon treatment with SGR was probed by confocal (D) and atomic force microscopy (E). Panel DI and DII (i, ii, iii) and panel EI (i, ii, iii) are images of intact nuclei. Panel EII (iv, v, vi) are AFM images upon MNase digestion. (i), (ii), and (iii) in (D, E) represent the untreated, DMSO-treated, and 5 μM SGR-treated cells. (iv), (v), and (vi) in (E) are MNase-digested images after similar treatments.

concentration (Figures 5C and 5D, compare lane 3 versus with 4–6). The inhibition of HAT-dependent in vitro chromatin transcription clearly indicates that SGR interacts with the physiological substrate chromatin and thereby blocks the histone acetylation, which is a prerequisite step for any transcription to occur from such a chromatin template.

Sanguinarine Treatment Modulates Global Gene Expression Differentially with Different Dosage

Sanguinarine inhibits histone-acetylation-dependent transcription and leads to the repression of the epigenetic modifications related to active transcription foci in vivo. These observations prompted us to investigate the effect of SGR in global gene

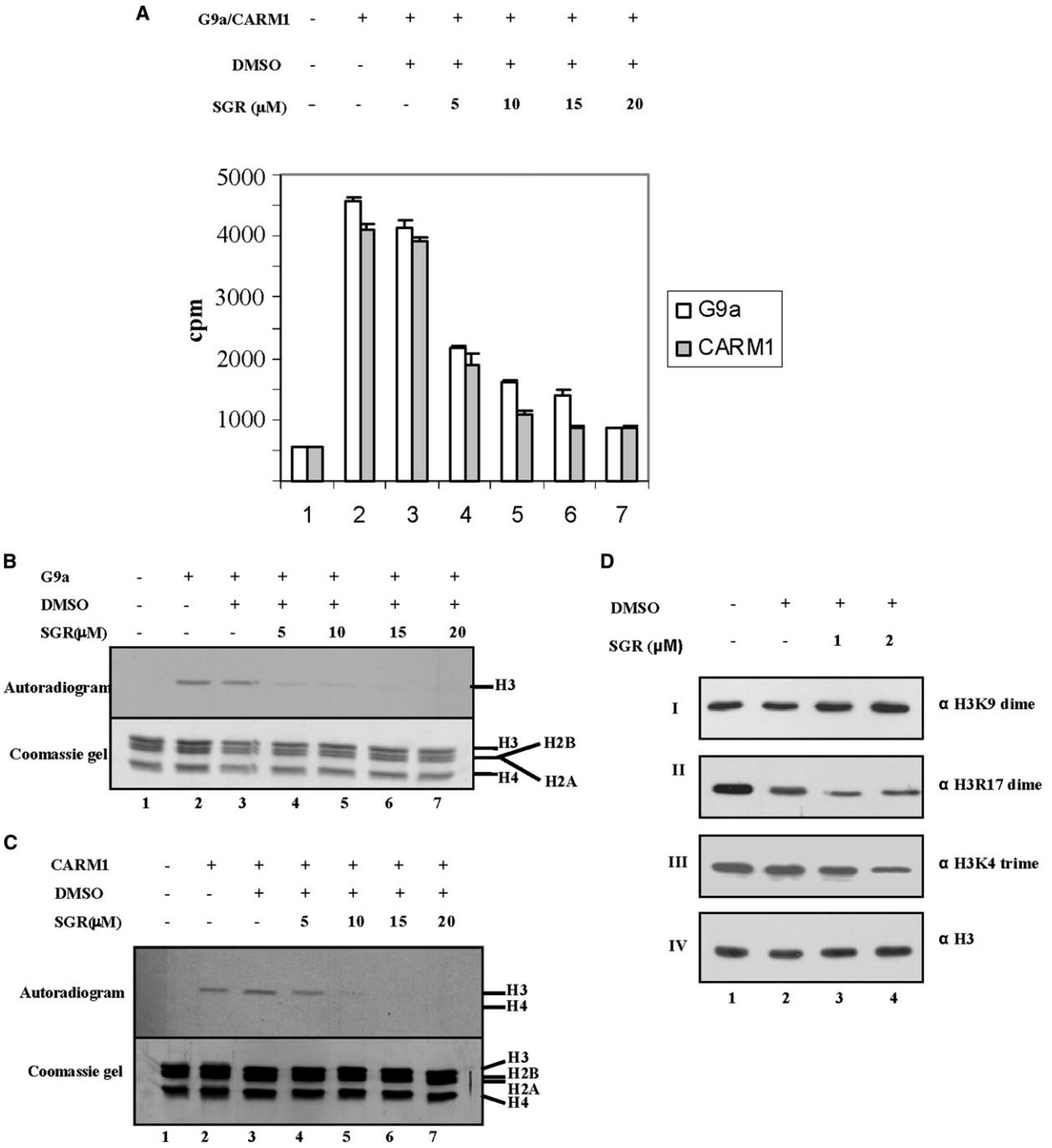

Figure 3. SGR Inhibits Histone Methylation

(A–C) HMTase assays were performed in the presence or absence of SGR using highly purified HeLa core histones (800 ng) and processed for filter binding (A) and gel assay fluorography (B, C). Lane 1, without any HMTase; lane 2, with HMTase; lane 3, with HMTase and in the presence of DMSO as solvent control; lanes 4–7, with HMTase and in the presence of 5, 10, 15, and 20 μM concentrations of SGR, respectively.

(D) Histones extracted from the compound-treated cells and subjected to western blotting analysis with antibodies against methylated H3K9 (I), H3R17 (II), and H3K4 (III) antibodies. Lane 1, untreated cells; lane 2, DMSO (solvent control) treated cells; lanes 3 and 4, 1 and 2 μM SGR-treated cells. Loading and transfer of equal amounts were confirmed by immunodetection of histone H3 (IV).

regulation. However, it is known that SGR induces apoptosis. Therefore, to investigate the probable effect of SGR mediated alteration of epigenetic marks and the subsequent global gene regulation, HeLa cells were treated with a 2 μM concentration of SGR for 3 hr. At this time point, the inhibition of histone acetylation becomes evident but apoptosis is not induced (Figure S3). Microarray hybridization of the treated samples revealed the expression of about 378 genes downregulated and 348 genes

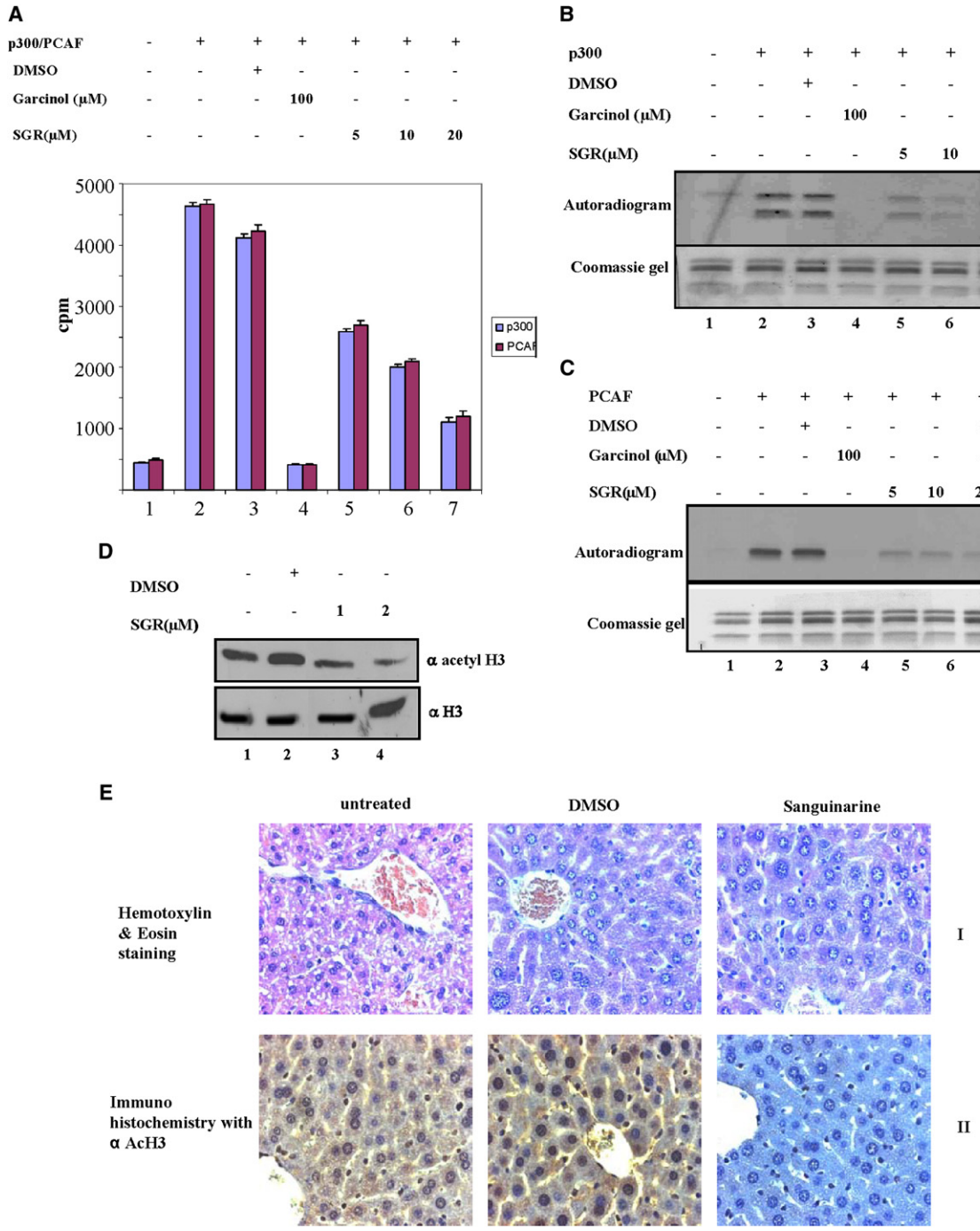

Figure 4. SGR Is a Potent Inhibitor of HATs

(A–C) Histone acetyltransferase assays were performed in the presence or absence of SGR using highly purified HeLa core histones (800 ng) and processed for filter binding (A) and gel assay fluorography (B, C). Lane 1, without any HAT; lane 2, with HAT; lane 3, with HAT and in the presence of DMSO as solvent control; lane 4, with HAT in the presence of garcinol (100 μM); lanes 5–7, with HAT and in the presence of 5, 10, 15, and 20 μM SGR respectively.

(D) Histones extracted from the compound treated cells and subjected to western blotting analysis with antibodies against acetylated histone H3. Lane 1, untreated cells; lane 2, DMSO (solvent control) treated cells; lanes 3 and 4, 1 and 2 μM SGR-treated cells. Loading and transfer of equal amounts were confirmed by immunodetection of histone H3.

(E) Upon treatment, mice liver tissue was processed for IHC analysis. Haematoxylin and eosin staining (I) and immunohistologic staining using acetylated histone H3 antibody (II) were performed.

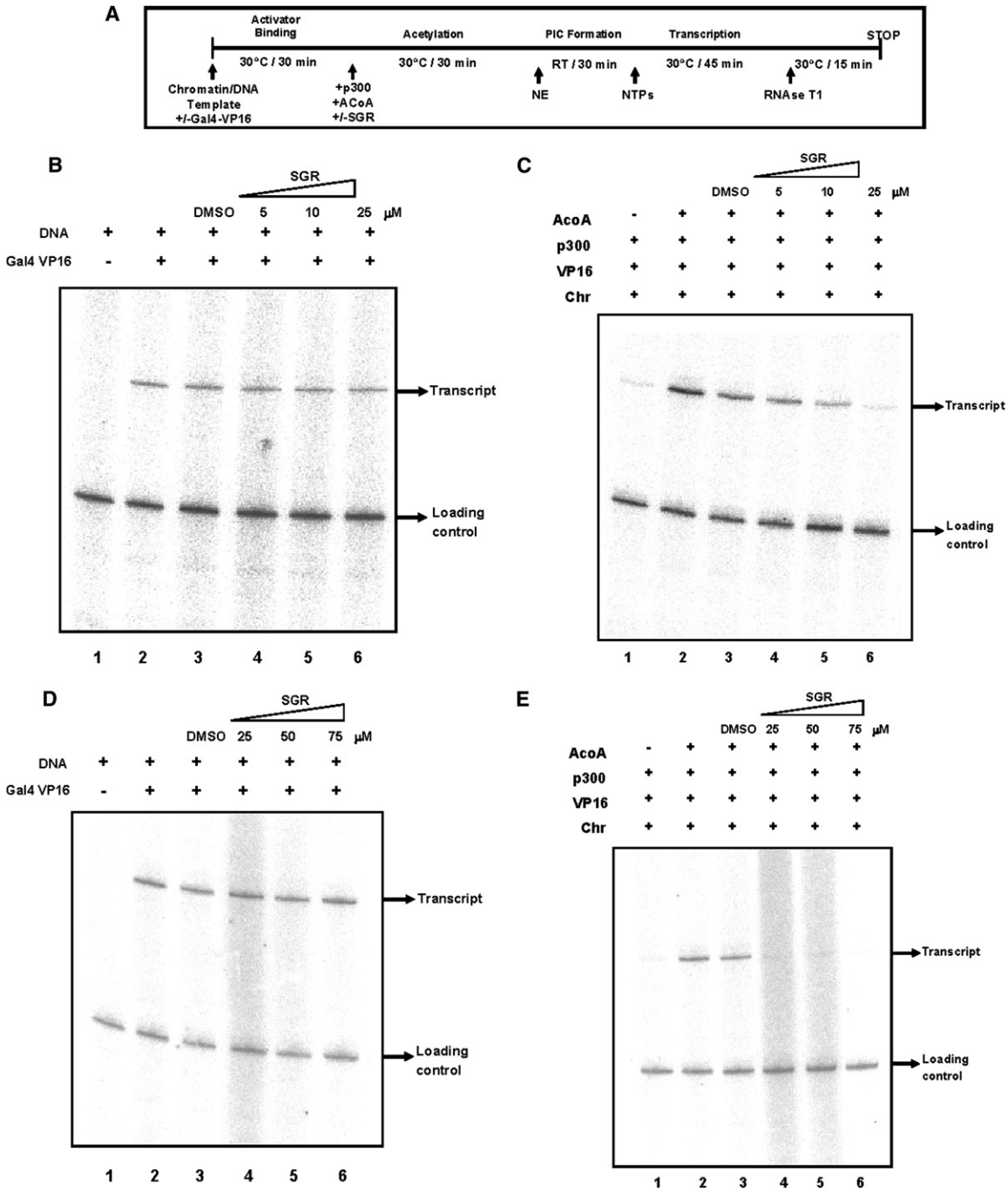

Figure 5. SGR Does Not Affect Transcription from DNA Template but Inhibits p300 Histone Acetyltransferase-Dependent Chromatin Transcription

(A–E) A schematic representation of in vitro transcription protocol. In vitro transcription from naked DNA template (B and D) and chromatin template (C and E). Freshly assembled chromatin template or equivalent amount of DNA (28 ng) was subjected to the protocol described in (A) with or without SGR. Lane 1, without activator (basal transcription); lane 2, with activator (Gal4-VP16); lane 3, with activator and DMSO; lanes 4–6, with activator and different concentration of SGR (as indicated).

upregulated (Figure 6A and Table S1). Among the upregulated genes, there was significant modulation of genes involved in cell signaling, focal adhesion, extracellular matrix (ECM) receptor interaction, and complement coagulation cascades. The genes that were downregulated were mostly from metabolic pathways, indicating an early event of metabolic downregulation on SGR treatment. Few representative genes were selected for the validation as represented in Figure 6B. Out of these, *CHFR3* (complement H related factor 3), a component of the complement system, was found to be significantly upregulated. One of the

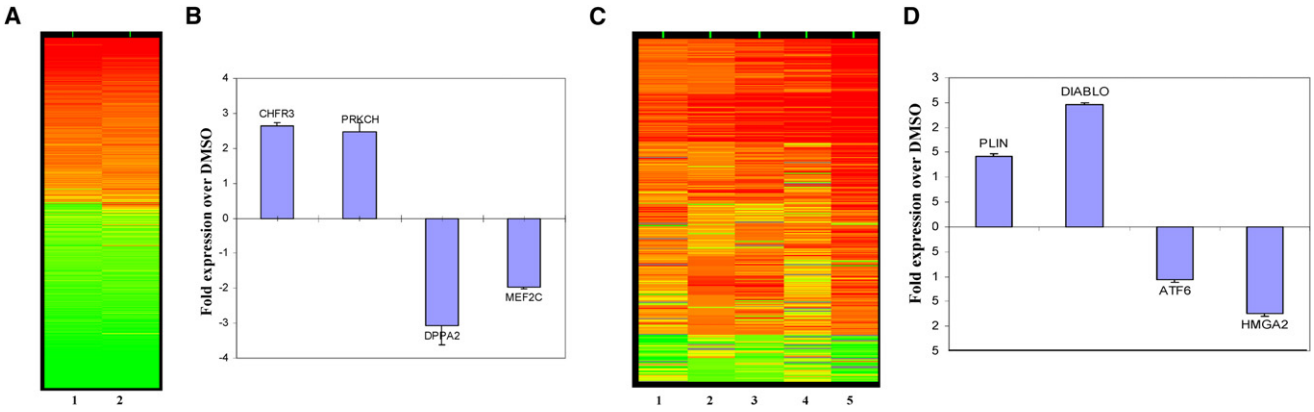

Figure 6. SGR Modulates Global Gene Expression

(A) Microarray analysis of gene expression upon treatment of HeLa cells with SGR. Lane 1 represents the forward reaction and lane 2 represents the dye swap.

(B) Validation of differentially altered genes by using real-time polymerase chain reaction (RT-PCR). *CHFR3* and *PRKCH* represent upregulated genes. *MEF2C* and *DPPA2* represent downregulated genes.

(C) Microarray analysis of gene expression upon treatment of HeLa cells with SGR. Lanes 1, 2, and 3 represent forward reaction, and lanes 4 and 5 represent dye swap.

(D) Validation of differentially altered genes by using RT-PCR. *PLIN* and *DIABLO* represent upregulated genes. *ATF6* and *HMGA2* represent downregulated genes.

components of the protein signaling cascade, *PRKCH* (protein kinase C), was also upregulated upon SGR treatment. However, an almost equivalent number of genes were also downregulated. *MEF2C* (myocyte enhancer factor 2), which itself is a transcription factor, was found to be downregulated. Another candidate gene, *DPPA2* (differentiation associated pluripotency protein), also showed downregulated expression with SGR treatment. The role of epigenetic modifications in SGR-mediated induction of apoptosis was further investigated by using a higher dosage of SGR (5 μM for 12 hr) and was followed by microarray analysis. However, the induction of apoptosis was confirmed by the expression of *Bax* (Figure S3). A total of 225 genes were upregulated and a very minor proportion of 35 genes were downregulated (Figure 6C) as a result of this treatment. The apoptosis-related genes were essentially upregulated (Table S2). The validation of the genes was done with few representative genes. (Figure 6D). *PLIN* (perilipin), a gene involved in lipid metabolism, was upregulated. Another important gene, *DIABLO* (direct IAP-binding protein with low pI), which is required for caspase activation for proper induction of apoptosis, was also significantly upregulated. Among the downregulated genes, *ATF6* (activating transcription factor), an ER-induced stress protein that gets attenuated during apoptosis, was downregulated. One of the nonhistone proteins involved with maintaining the structural architecture of chromatin, *HMGA2* (high mobility group protein A2), was also significantly downregulated, indicating the effect of SGR treatment on the structural integrity of chromatin as well. Taken together, these results suggest that apart from its role as an inducer of apoptosis and a DNA-damaging agent, SGR might also alter cellular homeostasis by modulating epigenetic marks through its direct interaction with chromatin.

DISCUSSION

In the present study, we have investigated both structural and functional consequences of interaction of the well-known putative anticancer therapeutic, SGR, with chromatin. Biophysical studies show that SGR, a well-known DNA-intercalating agent, can also bind to core histones. This dual-binding ability has been hitherto unreported for a DNA-binding putative anticancer agent. It induces radical structural alterations at both the mononucleosomal and chromatin level. Alteration at the mononucleosomal level is confined to an increase in its solvent-exposed surface area as a sequel to the unfolding of its structure. Such unfolding might be triggered by the dual-binding ability of SGR. However, SGR induces chromatin aggregation as indicated from circular dichroism, ITC, and dynamic light scattering measurements. The functional consequence of the dual-binding ability of SGR is manifested in its ability to inhibit the activity of histone acetyltransferases and histone methyltransferases, presumably through its direct interaction with core histones. Although SGR intercalates into DNA base pairs, it does not affect activator-dependent in vitro transcription from DNA template. However, emphasizing the functional importance of its inhibition of histone-modifying enzymes, it could inhibit acetylation-dependent chromatin transcription. In agreement with this phenomenon of involvement of the epigenetic mechanism, the global gene expression analysis with two different concentration of SGR treatment indicates a differential pattern. The preapoptotic stage indicates an almost equal upregulation and downregulation of gene expression due to the repression of epigenetic marks and the alteration of chromatin structure due to SGR interaction.

Observed blue shift of fluorescence peak in the steady-state fluorescence spectra could be due to either or both of the following processes: ground and/or excited-state stabilization of SGR and reduced dissipation of energy due to solvent interaction in the excited state of SGR upon intercalation. Extent of blue shift follows the order: chromatin > mononucleosome > chromosomal DNA (data not shown). This might be ascribed to the fact that solvent accessibility of SGR is least when it is bound to chromatin. As a result, energy dissipation due to solvent interaction in the excited state is also least for chromatin. On the other hand,

extent of energy dissipation enhances as a result of association with chromosomal DNA. However, the possibility of additional interaction with histones in stabilizing the ground state of SGR cannot be excluded. The analysis of excited-state fluorescence lifetimes of bound SGR provides an explanation. If energy dissipation due to solvent interaction of bound SGR for chromosomal DNA is the sole factor for the observed minimum blue shift of fluorescence maxima, then a lower excited-state lifetime for chromosomal DNA as compared with chromatin and mononucleosome could be expected. Interaction with chromosomal DNA exhibits maximum lifetime among the polymers. The apparent anomaly can be ascribed to the potential of the DNA intercalator to interact with histones within chromatin and mononucleosome. Results from fluorescence assays of SGR-core histone association (Figure 2B) reinforce the above fact.

Different stoichiometry values of SGR for the chromatin, mononucleosome and chromosomal DNA (Table 1) are similar to other DNA-binding drugs like chromomycin, mithramycin, and daunomycin (Mir and Dasgupta, 2001, and references therein). Negative ΔC_p values (Table 1) are proportional to the reduction in water-accessible nonpolar surface area of the ligand (Ortiz-Salmeron et al., 1998). The negative ΔC_p value of 90 $cal.mol^{-1}.K^{-1}$ for chromosomal DNA originates from the removal of water-accessible nonpolar ring structures of SGR from bulk solution to inside base pairs, when it intercalates into DNA base pairs. Higher magnitude of negative ΔC_p for chromatin relative to chromosomal DNA originates from aggregation of chromatin. The largest value of ΔC_p with opposite sign in case of mononucleosome occurs as a result of SGR-induced disruption of histone-DNA interaction. The dual-binding ability of SGR with DNA and core histones could be a potential cause of the disruption.

Analysis of CD spectra in the region of 310–380 nm suggests that the chiro-optical environments of the chromophore are different in chromatin, mononucleosome, and chromosomal DNA (Figure 2A). Differential position of the bielliptical positive induced band of polymer-bound SGR could be ascribed to local perturbation of binding mode by histones. This in turn gives rise to difference in binding site microenvironment and geometry after binding to chromatin and mononucleosome. Increase of positive CD signal at 272 nm could be ascribed to intercalation within DNA of native chromatin (Vergani et al., 1994). A control experiment with ethidium bromide (EtBr) showed an enhancement of molar ellipticity value from 3161 to 5283 (data not shown). Thus, binding of SGR can be expected to enhance the CD signal at 272 nm. In contrast, molar ellipticity value for chromatin at 272 nm decreases from 3161 to 2461 in the presence of SGR. The molar ellipticity value at 272 nm for chromatin shows a decrease with slow kinetics in the presence of SGR (inset of Figure 2A). Such a decrease in the CD band at 272 nm for chromatin is consistent with the proposition of SGR-induced chromatin aggregation (Das et al., 2006).

The effect of SGR upon size distribution of the chromatin, mononucleosome, and chromosomal DNA (Figure 2C) demonstrates that the alkaloid specifically aggregates chromatin. Confocal and atomic force microscopy results (Figure 2D, panels I and II; Figure 2E, panel I, compare i and ii with iii) show that chromatin aggregation leads to its compaction in the HeLa cells. AFM studies of isolated nuclei from HeLa cells subjected to partial MNase digestion indicate that SGR treatment leads to the formation of large compact chromatin domains that could be an indicative of transcriptional silencing (Figure 2E, panel II, compare iv and v with vi).

Sanguinarine is a potent inhibitor of histone-modifying enzymes in vitro. This can be explained by the general blocking of histones, thereby being inaccessible to the enzymes. The inhibition of histone methyltransferase activity by SGR is interesting. Although H3K9 methylation by G9a could be inhibited by SGR in vitro, this highly stable modification in the heterochromatin domain (Tachibana et al., 2001) was minimally affected by the presence of 2 μM SGR in vivo. This is expected because the modification within the cellular system (unlike the in vitro assays) does not occur as an exclusive event, but rather is modulated by other epigenetic marks and interacting proteins. Arginine methylation of H3R17, which along with histone acetylation sets the chromatin in an active state (Stallcup et al., 2000), was significantly reduced upon SGR treatment. Lysine methylation of H3K4, which is also associated with the transcriptionally active chromatin, was strongly inhibited by SGR. These observations suggest that SGR could inhibit the histone modifications in vitro by a general mechanism of binding to histones and making it unavailable for enzymatic activity. The kinetic analysis of SGR-mediated inhibition of the arginine methyltransferase CARM1 exhibits an uncompetitive mode of inhibition (Figure S4), indicating the involvement of the enzyme substrate complex in the inhibition. However, in the cells, SGR could alter the histone modifications that are transiently induced for activation associated gene expression more profoundly than those that are the more stable silent marks like H3K9 methylation, indicating a preference toward the transcriptionally active foci.

Sanguinarine could inhibit the HAT activity of p300 and PCAF potently, in vitro and in vivo. A previous report suggested that SGR is a potent inhibitor of the NF-κB pathway (Chaturvedi et al., 1997). Acetylation of one of the NF-κB subunits, p65, is essential for NF-κB activation (Chaturvedi et al., 1997). SGR might inhibit the acetylation of p65, thereby causing the inhibition of NF-κB activity. It is yet to be investigated whether SGR directly interacts with p300 and inhibits the acetyltransferase activity irrespective of the substrates (histones or nonhistones). The SGR inhibition kinetics with p300 exhibit a mixed type of inhibition with both the substrates (Figure S5). The result is preliminary evidence of the ability of SGR to bind to the enzyme, but the affinity of SGR is highly increased in the presence of the enzyme-substrate complex leading to a mixed inhibition. Thus, the kinetic analysis with both enzymes (CARM1 and p300) shows a clear indication toward the involvement of the substrate in the inhibition. Although SGR inhibited the activity of histone acetyltransferase, it does not inhibit histone deacetylase (HDAC1) activity (Figure S6). Interestingly, in both the enzymatic reactions, core histones are the common substrates, but the acetylated form is required for the deacetylation reaction. This indicates that SGR might not prefer to bind to the acetylated histones, and thus could not inhibit the HDAC1 activity. SGR is a potent DNA intercalator. Surprisingly, it could not affect the in vitro transcription from the DNA template even at 75 μM concentration. However, histone-acetylation-dependent chromatin transcription was strongly inhibited in a dose-dependent manner. These data suggest that through its histone interaction (and thereby HAT inhibitory ability), SGR might alter the global gene

expression pattern. Furthermore, SGR-mediated chromatin aggregation might also contribute to this process by reorganizing the chromatin territories (Fraser and Bickmore, 2007), which might also affect the gene expression globally.

Treatment of HeLa cells with 2 μM SGR for 3 hr (a dosage at which apoptosis is not induced) resulted in almost an equal upregulation and downregulation of genes. Inhibition of histone acetylation and H3R17 and H3K4 methylation by SGR could be attributed to the downregulation of gene expression. However, upregulation of gene expression might be caused by the alteration of chromatin organization (aggregation), and inhibition of a specific set of chromatin-modifying enzyme activity. Furthermore, under specific consequences, p300 might also induce transcriptional repression (Mantelingu et al., 2007, Sankar et al., 2008). The functional genes are present in a three-dimensional microenvironment (chromatin territories), and any alteration of this structural organization might lead to the exposure of the buried regions to the transcriptionally active foci, resulting in gene expression. Many candidate genes of the cell communication pathway like collagen, keratin, and vitronectin were upregulated. These genes have a role in ECM receptor interaction and in focal adhesion. This indicates that the early event in SGR treatment might be targeted toward the extracellular regions. However, kinases like PRKCE and SOCS, which are suppressors of cytokine signaling, were also upregulated, indicating the physiological activation of signaling process. By contrast, the downregulated genes were mostly members of metabolic pathways, which is an implication on the early effect of SGR on important metabolic processes because of its modulation of chromatin modifications and not due to any interaction with cellular components. This phenomenon was verified by an in vitro assay with an important metabolic, nonchromatin enzyme GAPDH (glyceraldehyde-3-phosphate dehydrogenase). SGR did not affect the dehydrogenase activity of GAPDH even at 50 μM concentration as observed from the absorbance values (Figure S7, lanes 3–7). However, garcinol, a potent apoptosis-inducing agent that is known to affect important metabolic pathways (Balasubramanyam et al., 2004a), could inhibit the dehydrogenase activity of GAPDH completely at 50 μM concentration (Figure S7, lane 8).

Microarray analysis of 5 μM SGR-treated HeLa cells resulted in a large upregulation of genes (225), whereas 36 genes were found to be downregulated. The upregulation of several genes upon SGR treatment was not quite surprising, as previous reports suggest that SGR induces DNA damage as well as apoptosis. Apart from these evidences, this could also be an effect of the physical alteration of chromatin structure by SGR (as discussed above). The downregulation of *HMGA2* is an indication of the loss of the structural proteins of chromatin. However, downregulation of genes in presence of SGR could be due to the inhibition of chromatin modifications (especially acetylation). Among the upregulated genes, many play a role in DNA repair. Therefore, these results confirm that SGR indeed targets DNA and causes its damage. Many genes involved in cell growth, differentiation, and morphogenesis were upregulated. SGR was known to cause cell death in numerous cancer cell lines through the accumulation of CyclinD1 and topoisomerase II in cytoplasm (Holy et al., 2006). Our results indeed show the upregulation of topoisomerase II as one of the candidate genes. Among the downregulated genes, many are involved in cell growth, gene regulation, and various cancers. *Rab3* (a member of RAS oncogene family) levels, which are elevated in various cancers, was downregulated upon SGR treatment. Modulation of arachidonic acid metabolism is a novel target for cancer therapy. Cytochrome P450, which plays a crucial role in the arachidonic acid pathway, was downregulated in our microarray analysis. Representative genes that were validated were specifically modulated by p300 in our previous work on a specific inhibitor of p300 (Mantelingu et al., 2007). The upregulation of *PLIN* and *DIABLO*, and the downregulation of *ATF6* and *HMGA2*, are similar to p300-specific inhibition. These data clearly indicate the dual mechanism of an SGR-mediated anticancer effect wherein the epigenetic mode of repression is functional at an early preapoptotic stage along with the later event of apoptosis induction. This mode of action might be similar for all DNA-binding drugs that also interact with chromatin.

In order to understand the mechanism of action of this important plant alkaloid as a putative anticancer compound, it would be essential to consider the interactions of SGR with the dynamic chromatin components and the subsequent alterations of post-translational modifications of histones and nonhistone proteins. However, derivatization of SGR and related alkaloids could be useful to design more specific and relatively less cytotoxic antineoplastic therapeutics, which could act on chromatin modifications in a more targeted manner.

SIGNIFICANCE

In this report, we show that SGR, a putative anticancer DNA intercalator, interacts not only with DNA but also with histones. SGR inhibits important chromatin modifications like acetylation and methylation. Remarkably, SGR could inhibit the transcription from chromatin template but not DNA. In vivo, SGR modulates the expression of a large number of genes differentially based on dosage. It exhibits a dual mechanism of action, wherein the initial effects are due to the alteration of the epigenetic marks. The secondary effects are due to SGR-mediated activation of the apoptotic pathway. These results establish a unique perspective of DNA-binding drugs and demand a new set of investigations about these compounds regarding their effect on epigenetic alterations. These data would be highly useful in understanding the mechanism of action of anticancer drugs as well as in designing new-generation therapeutics.

EXPERIMENTAL PROCEDURES

Preparation of Chromatin and Mononucleosome from Rat Liver

Male albino Sprague-Dawley rats weighing about 150 ± 10 g and about 2 or 3 months old were used throughout this study. Nuclei were isolated from the homogenized liver by using a standard method described elsewhere (Blobel and Potter, 1966; Burton., 1956).

Preparation of Chromatin from HeLa Cells

Chromatin from HeLa cells was isolated by using a standard method described elsewhere (Das et al., 2006).

Absorbance and Fluorescence Measurement

Absorption spectra were recorded with a CECIL 7500 spectrophotometer. The concentration of SGR in 10 mM Na-acetate (pH 5.2) was estimated with the molar absorption coefficient (ε) of 30,700 $M^{-1}cm^{-1}$ at 327 nm. Fluorescence

measurements were performed with a PerkinElmer LS55 luminescence spectrometer using 1 cm path length quartz cuvettes. Excitation and emission slits with a band pass of 5 nm and 10 nm, respectively, were used for all measurements. During fluorescence measurements, absorbance of the samples did not exceed 0.05 at 327 nm. Therefore, we did not correct the emission intensity for optical filtering effect. The excitation and emission wavelengths were 327 and 570 nm, respectively.

Fluorescence Lifetime Measurements

Fluorescence lifetimes were calculated from time-resolved fluorescence decays using a luminescence spectrophotometer (Edinburgh Instruments Ltd., Scotland) in the time-correlated single photon counting mode. The excitation source is a nanosecond flash lamp filled with nitrogen as plasma gas. Lamp profiles were measured at the excitation wavelength (327 nm) using Ludox (colloidal silica) as the scatterer. For each measurement, 3000 photon counts were collected in the peak channel. All experiments were performed using excitation and emission slits with a nominal band pass of 4 nm. Intensity decay curves were fitted as a sum of exponential terms:

$$F(t) = \sum_i \alpha_i \exp(-t/\tau_i)$$

where α_i is a pre-exponential factor representing the fractional contribution to the time-resolved decay of the component with a lifetime τ_i. The decay parameters were recovered using a nonlinear least-squares iterative fitting procedures based on the Marquardt algorithm (Bevington, 1969). The goodness of fit of a given set of observed data and the chosen function was evaluated by the reduced χ^2 value not more than 1.5. Mean (average) lifetime $<\tau>$ for biexponential decays of fluorescence was calculated from the decay times and pre-exponential factors using the following equation (Lakowich, 1999):

$$<\tau> = \frac{\alpha 1 \tau 1^2 + \alpha 2 \tau 2^2}{\alpha 1 \tau 1 + \alpha 2 \tau 2}$$

Circular Dichroic Spectroscopy

Circular dichroism measurements were done in a JASCO J-720 spectropolarimeter (Jasco Corporation, Tokyo, Japan) at 25°C equipped with a temperature controller. The CD scans were recorded within the wavelength range of 200–400 nm at sensitivity set to 10 mdeg and scan speed 20 nm per minute with step size of 0.5 nm. The time constant was 1 s and bandwidth was 0.2 nm. All measurements were done in a cuvette of 1 cm path length in a reaction volume of 2 ml in 10 mM Tris-HCl (pH 6.5) at 25°C. In a reaction mixture containing 10 μM SGR, individual titration was performed with different levels of chromatin structure (polymers) to achieve a concentration range of 2.8 to 39 μM. The reaction mixture was incubated for 2 min before scanning. All spectra are average of three runs. They were smoothed within the permissible limits by the inbuilt software of the instrument.

Isothermal Titration Calorimetry

Isothermal calorimetric measurements were performed in a VP-ITC microcalorimeter (Microcal Inc.) at different temperatures between 10°C to 30°C. Samples were centrifuged and degassed before titration. Titration of SGR against different levels of chromatin structure was performed by injecting polymers into SGR. A blank experiment in which polymers were injected into buffer with no SGR was done to correct the data due to dilution. Background was subtracted from the measured heats, and the corrected heats were plotted against molar ratio and analyzed using manufacturer's software yielding the stoichiometry n (in terms of number of bases/drug molecule), equilibrium dissociation constant ($K_d = 1/K_a$), and enthalpy (ΔH). From the relationship $\Delta G^\circ = -RT \ln K_a$ and the Gibbs-Helmholtz equation, the entropy of association (ΔS) was calculated. Change in heat capacity (ΔC_p) for the association of SGR with different polymers was calculated from the plot of enthalpy change (ΔH) against temperature.

Dynamic Light Scattering

Dynamic light scattering experiments were performed using the Zetasizer Nanoseries (Malvern Instruments) equipped with a 4 mW He-Ne laser (λ = 632 nm). This instrument measures the fluctuation in scattering intensity and uses this to determine the diffusion coefficient, Q, of the sample by means of its inbuilt autocorrelator. Size of the particles is calculated using Stokes-Einstein equation:

$$D_H = \frac{kT}{f} = \frac{kT}{3\pi\eta Q}$$

where D_H is the hydrodynamic diameter, k is the Boltzmann constant, f is particle frictional coefficient, η is solvent viscosity (here, we have given the viscosity of water as the solvent viscosity), T is the absolute temperature, and Q is the diffusion coefficient.

Binding Analysis

Results from fluorimetric titrations were analyzed with a standard method described elsewhere (Mir and Dasgupta, 2001). Binding stoichiometry (expressed in terms of site size) was estimated from the intersection of the two straight lines of a least-squares fit plot of normalized change in fluorescence against the input concentration of the polymer.

Confocal Microscopy

HeLa cells were cultured as monolayer on the poly-L-lysine-coated coverslips in Dulbecco's minimal essential medium (Sigma). SGR-treated (2 μM) cells were then fixed. Nuclear staining of fixed cells was done with Hoechst 33258 (Sigma). Images were taken with a Zeiss LSM 510 META confocal microscope.

Atomic Force Microscopy

Nuclei were isolated from SGR-treated (2 μM) HeLa cells as described elsewhere. After subjecting the nucleus to MNase digestion, samples were fixed and dried for AFM visualization. AFM observation was performed with a Bioscope/Bioscope SZ; Nanoscope IIIa controller (Veeco Instruments Inc., Santa Barbara, CA, USA) using the contact mode. The cantilever (nonconductive silicon nitride, Veeco model DNP-20) was in 0.4–0.7 mm long with a spring constant of 0.06 N/m. The scanning frequency was 1.001 Hz, and images are captured with the height mode in a 256 × 256 and 512 × 512 pixel format.

Purification of Human Core Histones and Recombinant Proteins

Human core histones were purified from HeLa nuclear pellet as described previously (Kundu et al., 1999). Purification of recombinant p300, G9a, CARM-1, PCAF, HDAC1, NAP1, and Gal4-VP16 was performed as described elsewhere (Kundu et al., 2000, Balasubramanyam et al., 2004a, 2004b).

Histone Acetyltransferase and Deacetylase Assay

The HAT and HDAC assays were performed as described previously (Kundu et al., 2000, Balasubramanyam et al., 2004a, 2004b).

Analysis of In Vivo Histone Acetylation

The histone modification analysis in the HeLa cells on SGR treatment was done as described previously (Mantelingu et al., 2007). For the animal experiment, SGR 25 mg/kg body weight in 50 μl DMSO was injected to mice, which were killed after 6 hr. Mice liver tissue was processed for paraffin embedding followed by microtome sectioning and processing for immunohistochemical staining with acetylated histone H3 antibody.

Histone Methyltransferase Assays

Histone methyltransferase assays were performed in a 30 μl reaction. The reaction mixture containing highly purified HeLa core histones, with or without histone methyltransferases in the HMT assay buffer 20 mM Tris, 4 mM EDTA (pH 8.0), 200 mM NaCl, along with varying concentrations of SGR for 10 min at 30°C. After the initial incubation, 1 μl 15 Ci/mmol [^{3}H] (S)-adenosyl methionine (Amersham) was added to the reaction mixtures, and the incubation continued for 15 min. The reaction mixture was then blotted onto P-81 (Whatman) filter paper, and radioactive counts were recorded on a PerkinElmer Wallac 1409 liquid scintillation counter. The reaction products were TCA precipitated, resolved on 15% SDS-PAGE, and subjected to fluorography followed by autoradiography.

Analysis of In Vivo Histone Methylation

The histone modification analysis in the HeLa cells on SGR treatment was done as described previously (Mantelingu et al., 2007), using the following

antibodies: dimethylated H3K9 (Upstate), asymmetric dimethylated H3R17 (Upstate), and trimethylated H3K4 (Upstate).

In Vitro Transcription

DNA and chromatin transcription assays were performed as described earlier with minor modifications (Kundu et al., 2000, Balasubramanyam et al., 2004a, 2004b).

Microarray Analysis

HeLa cells were treated with the indicated concentration of SGR (2 μM or 5 μM). The DMSO-treated cells were used as control. RNA was isolated after the indicated time of treatment (3 hr or 12 hr, respectively). The 2 μM treated samples were hybridized on Agilent human 15K whole genome array. The 5 μM treated samples were hybridized on Toronto human 19K whole genome array. Data analysis was done using GeneSpring software. The normalization was done using GeneSpring GX using the recommended per spot, per chip intensity dependent (lowest) normalization.

Endogenous Gene Expression Assay by Real-Time Polymerase Chain Reaction Analysis

HeLa cells were treated with SGR for the indicated time point with the indicated concentration. DMSO-treated cells were used as controls. Following the stipulated time of treatment, the total RNA was isolated using Trizol reagent (Invitrogen). The cDNA was amplified with oligo dT (28-mer) (Invitrogen) by MMLV reverse transcriptase (Sigma), and the expression analysis was done with the help of iQTM SyBR green supermix (Bio-Rad) and gene-specific primers of actin and *CHFR3* (forward primer: 5′- TGGGTTTCCTGTGCTAATG-3′, reverse primer: 5′-AGTCTCAAAATGTTCATCAC-3′), *PRKCH* (forward primer: 5′-GAAAAGTCCCACGGAGGAG-3′, reverse primer: 5′-TGCTTCGCAGCGGGAGAACCG-3′), *MEF2C* (forward primer: 5′-CTGCATGTTTGAATCAGGTG-3′, reverse primer: 5′-ATTCGTTCCTGATGAAGGAAG-3′), *DPPA2* (forward primer: 5′-ATCAACTTGATGAAGGAAG-3′, reverse primer: 5′-ATCCAAATTTGCATCTGAC-3′), *DIABLO* (forward primer: 5′-CAGAGGAGGAAGATGAAGTG-3′, reverse primer: 5′-CAATCCTCACGCAGGTAGGC-3′), *PLIN* (forward primer: 5′-CAGGAGAATGTGCTGCAGCG-3′, reverse primer, 5′-AGGCGGGTGGAGATGGTGTC-3′), *ATF6* (forward primer: 5′-GACTCTTTCACAGGCTGGA-3′, reverse primer: 5′-CTTCCTTCAGTGGCTCCGC-3′), *HMGA2* (forward primer, 5′-ATGAGCGCACGCGGTGAG-3′, reverse primer: 5′-GTGATCCTCTTCGGCAGAC-3′).

For technical details regarding the DLS studies, HDAC assay, in vitro transcription, purification of human core histones, and other recombinant proteins, please refer to Supplemental Experimental Procedures.

ACCESSION NUMBER

Guidelines set by MIAME were followed, and the raw microarray data have been deposited in NCBI's Gene Expression Omnibus (http://www.ncbi.nlm.nih.gov/geo/query/acc.cgi?acc=GSE14314) and are accessible through GEO Series accession number GSE14314 and GSE14777.

SUPPLEMENTAL DATA

The Supplemental Data include Supplemental Experimental Procedures, Supplemental References, seven figures, and two tables and can be found with this article online at http://www.cell.com/chemistry-biology/supplemental/S1074-5521(09)00004-0.

ACKNOWLEDGMENTS

We thank G. Sureshkumar, Indian Institute of Chemical Biology, Kolkata for the gift of SGR during the initial phase of the work. This work is supported by the Department of Atomic Energy, Government of India, and Jawaharlal Nehru Centre for Advanced Scientific Research. We acknowledge the Confocal Microscopy facility of Molecular Biology and Genetics Unit, JNCASR. R.S., J.S., and S.G. are senior research fellows of CSIR, Government of India. We also acknowledge Chemical Sciences Division, SINP, Kolkata for fluorescence lifetime and CD measurements. We thank Anjan K. Dasgupta and S.S. Sinha, Department of Biochemistry, Calcutta University, for technical assistance during the DLS measurements.

Received: September 12, 2008
Revised: December 5, 2008
Accepted: December 29, 2008
Published: February 26, 2009

REFERENCES

Adhami, V.M., Aziz, M.H., Mukhtar, H., and Ahmad, N. (2003). Activation of prodeath Bcl-2 family proteins and mitochondrial apoptosis pathway by SGR in immortalized human HaCaT keratinocytes. Clin. Cancer Res. *9*, 3176–3182.

Adhami, V.M., Aziz, M.H., Reagan-Shaw, S.R., Nihal, M., Mukhtar, H., and Ahmad, N. (2004). SGR causes cell cycle blockade and apoptosis of human prostate carcinoma cells via modulation of cyclin kinase inhibitor-cyclin dependent kinase machinery. Mol. Cancer Ther. *3*, 933–940.

Balasubramanyam, K., Altaf, M., Varier, R.A., Swaminathan, V., Ravindran, A., Sadhale, P.P., and Kundu, T.K. (2004a). Polyisoprenylated benzophenone, garcinol, a natural histone acetyltransferase inhibitor, represses chromatin transcription and alters global gene expression. J. Biol. Chem. *279*, 33716–33726.

Balasubramanyam, K., Varier, R.A., Altaf, M., et al. (2004b). Curcumin, a novel p300/CREB-binding protein-specific inhibitor of acetyltransferase, represses the acetylation of histone/nonhistone proteins and histone acetyltransferase-dependent chromatin transcription. J. Biol. Chem. *279*, 51163–51171.

Barreto, M.C., Pinto, R.E., Arrabaca, J.D., and Pavao, M.L. (2003). Inhibition of mouse liver respiration by chelidinium majus isoquinoline alkaloids. Toxicol. Lett. *146*, 37–47.

Bevington, P.R. (1969). Data Reduction and Error Analysis for the Physical Sciences (New York: McGraw-Hill).

Blobel, G., and Potter, V.R. (1966). Nuclei from rat liver: isolation method that combines purity and high yield. Science *154*, 1662–1665.

Burton, K. (1956). A study of the conditions and mechanism of the diphenylamine reaction for the colorimetric estimation of deoxyribonucleic. Biochem. J. *62*, 315–323.

Chaturvedi, M.M., Kumar, A., Darnay, B.G., Chainy, G.B., Agarwal, S., and Aggarwal, B.B. (1997). SGR (pseudochelerythrine) is a potent inhibitor of NF-kappaB activation, IkappaBalpha phosphorylation, and degradation. J. Biol. Chem. *272*, 30129–30134.

Das, C., Hizume, K., Batta, K., Kumar, B.R., Gadad, S.S., Ganguly, S., Sadhale, P.P., Takeyasu, K., and Kundu, T.K. (2006). Transcriptional coactivator PC4, a chromatin-associated protein, induces chromatin condensation. Mol. Cell. Biol. *26*, 8303–8315.

Das, S., Kumar, G.S., and Maiti, M. (2003). Spectroscopic and thermodynamic studies on the binding of SGR and berberine to triple and double helical DNA and RNA structures. J. Biomol. Struct. Dyn. *20*, 703–714.

Dvorak, Z., and Simanek, V. (2007). Metabolism of sanguinarine: the facts and the myths. Curr. Drug Metab. *8*, 173–176.

Fraser, P., and Bickmore, W. (2007). Nuclear organization of the genome and the potential for gene regulation. Nature *447*, 413–417.

Hogan, C., and Varga-Weisz, P. (2007). The regulation of ATP-dependent nucleosome remodelling factors. Mutat. Res. *618*, 41–51.

Holy, J., Lamont, G., and Perkins, E. (2006). Disruption of nucleocytoplasmic trafficking of cyclin D1 and topoisomerase II by sanguinarine. BMC Cell Biol. *7*, 13.

Hussain, A.R., Al-Jomah, N.A., Siraj, A.K., Manogaran, R., Al-Hussain, K., Abubaker, J., Platanias, L.C., Al-Kuraya, K.S., and Uddin, S. (2007). SGR-dependent induction of apoptosis in primary effusion lymphoma cells. Cancer Res. *67*, 3888–3897.

Jones, P.A., and Baylin, S.B. (2007). The epigenomics of cancer. Cell *128*, 683–692.

Kouzarides, T. (2007). Chromatin modifications and their function. Cell *128*, 693–705.

Kundu, T.K., Wang, Z., and Roeder, R.G. (1999). Human TFIIIC relieves chromatin-mediated repression of RNA polymerase III transcription and contains an intrinsic histone acetyltransferase activity. Mol. Cell. Biol. *19*, 1605–1615.

Kundu, T.K., Palhan, V.B., Wang, Z., An, W., Cole, P.A., and Roeder, R.G. (2000). Activator-dependent transcription from chromatin in vitro involving targeted histone acetylation by p300. Mol. Cell *6*, 551–561.

Lakowich, J.R. (1999). Principles of Fluorescence Spectroscopy (New York: Kluwer-Plenum Press).

Maiti, M., and Kumar, G.S. (2007). Molecular aspects on the interaction of protoberberine, benzophenanthridine and aristolochia group of alkaloids with nucleic acid structures and biological perspectives. Med. Res. Rev. *27*, 649–695.

Maiti, M., Das, S., Sen, A., Das, A., Kumar, S.G., and Nandi, R. (2002). Influence of DNA structures on the conversion of SGR alkanolamine form to iminium form. J. Biomol. Struct. Dyn. *20*, 455–466.

Malikova, J., Zdarilova, A., and Hlobilkova, A. (2006). Effects of SGR and chelerythrine on the cell cycle and apoptosis. Biomed. Pap. Med. Fac. Univ. Palacky Olomouc Czech Repub. *150*, 5–12.

Mandel, I.D. (1994). Antimicrobial mouthrinses: overview and update. J. Am. Dent. Assoc. *125* (*Suppl 2*), 2S–10S.

Mantelingu, K., Reddy, B.A., Swaminathan, V., Kishore, A.H., Siddappa, N.B., Kumar, G.V., Nagashankar, G., Natesh, N., Roy, S., Sadhale, P.P., et al. (2007). Specific inhibition of p300-HAT alters global gene expression and represses HIV replication. Chem. Biol. *14*, 645–657.

Mir, M.A., and Dasgupta, D. (2001). Interaction of antitumor drug, mithramycin with chromatin. Biochem. Biophys. Res. Commun. *280*, 68–74.

Murcia, G., Das, G., Erard, M., and Daune, M. (1978). Superstructure and CD spectrum as probe of chromatin integrity. Nucleic Acids Res. *5*, 523–535.

Nakagawa, M., Oda, Y., Eguchi, T., Aishima, S., Yao, T., Hosoi, F., Basaki, Y., Ono, M., Kuwano, M., Tanaka, M., and Tsuneyoshi, M. (2007). Expression profile of class I histone deacetylases in human cancer tissues. Oncol. Rep. *18*, 769–774.

Oki, M., Aihara, H., and Ito, T. (2007). Role of histone phosphorylation in chromatin dynamics and its implications in diseases. In Chromatin and Disease, T.K. Kundu and D. Dasgupta, eds. (Dordrecht, The Netherlands: Springer), pp. 319–336.

Ortiz-Salmeron, E., Baron, C., and Garica-Fuentes, L. (1998). Enthalpy of captopril-angiotensin I-converting enzyme binding. FEBS Lett. *435*, 219–224.

Prendergast, F.G. (1991). Time-resolved fluorescence techniques: methods and applications in biology. Curr. Opin. Struct. Biol. *1*, 1054–1059.

Rothhammer, T., and Bosserhoff, A.K. (2007). Epigenetic events in malignant melanoma. Pigment Cell Res. *20*, 92–111.

Sankar, N., Baluchamy, S., Kadeppagari, R.K., Singhal, G., Weitzman, S., and Thimmapaya, B. (2008). p300 provides a corepressor function by cooperating with YY1 and HDAC3 to repress c-Myc. Oncogene *27*, 5717–5728.

Shamma, M., and Guinaudeau, H. (1986). Aporphinoid alkaloids. Nat. Prod. Rep. *3*, 345–351.

Stallcup, M.R., Chen, D., Koh, S.S., Ma, H., Lee, Y.H., Schurter, B.T., and Aswad, D.W. (2000). Co-operation between protein-acetylating and protein-methylating co-activators in transcriptional activation. Biochem. Soc. Trans. *28*, 415–418.

Straub, K.D., and Carver, P. (1975). SGR, inhibitor of Na-K dependent ATPase. Biochem. Biophys. Res. Commun. *62*, 913–922.

Swaminathan, V., Reddy, B.A., Ruthrotha Selvi, B., Sukanya, M.S., and Kundu, T.K. (2007). Small molecule modulators in epigenetics: implications in gene expression and therapeutics. In Chromatin and Disease, T.K. Kundu and D. Dasgupta, eds. (Dordrecht, The Netherlands: Springer), pp. 397–428.

Tachibana, M., Sugimoto, K., Fukushima, T., and Shinkai, Y. (2001). Set domain-containing protein, G9a, is a novel lysine-preferring mammalian histone methyltransferase with hyperactivity and specific selectivity to lysines 9 and 27 of histone H3. J. Biol. Chem. *276*, 25309–25317.

Tonini, T., D'Andrilli, G., Fucito, A., Gaspa, L., and Bagella, L. (2008). Importance of Ezh2 polycomb protein in tumorigenesis process interfering with the pathway of growth suppressive key elements. J. Cell. Physiol. *214*, 295–300.

Ulrichova, J., Dvorak, Z., Vicra, J., Lata, J., Smrzova, J., Sedo, A., and Somanek, V. (2001). Cytoyoxicity of natural compound in hepatocyte cell culture models. The case of quaternary benzo[c]phenanthridine alkaloids. Toxicol. Lett. *125*, 125–132.

Vallejos, R.H. (1973). Uncoupling photosynthetic phosphorylation by benzophenanthridine alkaloid. Biochem. Biophys. Acta *292*, 193–196.

Van Beekum, O., and Kalkhoven, E. (2007). Aberrant forms of histone acetyltransferases in human disease. In Chromatin and Disease, T.K. Kundu and D. Dasgupta, eds. (Dordrecht, The Netherlands: Springer), pp. 233–262.

Vergani, L., Gavazzo, P., Mascetti, G., and Nicolini, C. (1994). Ethidium bromide intercalation and chromatin structure: a spectropolarimetric analysis. Anal. Biochem. *33*, 6578–6585.

Vogt, A., Tamewitz, A., Skoko, J., Sikorski, R.P., Giuliano, K.A., and Lazo, J.S. (2005). The benzo[c]phenanthridine alkaloid, SGR, is a selective, cell-active inhibitor of mitogen activated protein kinase phosphatase-I. J. Biol. Chem. *280*, 19078–19086.

Wang, B.H., Lu, Z.X., and Polya, G.M. (1997). Inhibition of eukaryotic protein kinase by isoquinoline and oxazine alkaloids. Planta Med. *63*, 494–498.

Wolff, J., and Knipling, L. (1993). Antimicrotubule properties of benzophenanthridine alkaloids. Biochemistry *32*, 13334–13339.